Enhancement of Pd Catalytic Activity toward Ethanol Electrooxidation by Atomic Layer Deposition of SnO2 onto TiO2 Nanotubes

Maïssa Barr, Loïc Assaud, Nicolas Brazeau, Margrit Hanbücken, Spyridon Ntais, Lionel Santinacci, Elena Baranova

Enhancement of Pd Catalytic Activity Toward Ethanol Electrooxidation By Atomic Layer Deposition of SnO_2 onto TiO_2 Nanotubes

Maïssa K. S. Barr,[†] Loïc Assaud,[†,‡] Nicolas Brazeau,[#] Margrit Hanbücken,[†] Spyridon Ntais,[#] Lionel Santinacci,[†,*] and Elena A. Baranova[#,*]

[†]*Aix Marseille Univ, CNRS, CINaM, Marseille, France*

[‡]*Institut de Chimie Moléculaire et des Matériaux d'Orsay, Université Paris-Sud/Université Paris-Saclay, CNRS, Rue du Doyen Georges Poitou, F-91405 Orsay, France*

[#]*Department of Chemical and Biological Engineering, Centre for Catalysis Research and Innovation, University of Ottawa, 161 Louis-Pasteur St., Ottawa, ON, K1N 6N5, Canada*

ABSTRACT. Palladium nanoparticles and SnO_2 layers have been grown by two successive steps of atomic layer deposition onto TiO_2 nanotubes (TNTs). The three-dimensional nanostructured catalytic systems have been studied for ethanol electrooxidation in alkaline media. Characterization by scanning and transmission electron microscopies, x-ray photoelectron spectroscopy, and x-ray diffraction indicates the high conformity, the high purity, and the perfect stoichiometry of Pd and SnO_2 deposits onto the TNTs. The electrochemical investigations performed by cyclic voltammetry and chronoamperometry have revealed the beneficial effect of the annealing of the support toward ethanol electrooxidation reaction. The comparison of the catalytic activity with literature shows that such SnO_2 based substrates exhibits highly promising performances.

INTRODUCTION

Direct alcohol fuel cells (DAFCs) have received a great deal of attention for energy generation and storage in portable electronic devices and vehicles. Among the different possible alcohols, ethanol is a promising liquid fuel because it has no toxicity, a high energy density and it can be easily produced from the fermentation of biomass.[1-3] However, the ethanol oxidation kinetics on Pt-based catalysts in acidic media is slow, incomplete and mostly leads to the production of acetic acid and acetaldehyde. The recent development of anion exchange solid electrolytes advanced the development of alkaline DAFCs where the oxidation kinetics is faster and allows using cheaper electrocatalysts than Pt. Pt-free catalysts or Pt alloying with co-catalysts can be used for ethanol oxidation reaction (EOR) in alkaline media.[4] Within this context, palladium has emerged as an attractive candidate for DAFCs. Pd is more abundant and less expensive, however the EOR is not complete in alkaline media leading to acetate and acetaldehyde formation in addition to small amounts of CO_2. It is therefore necessary to improve the catalyst to efficiently break the C–C bond at low overpotentials. In order to improve the performances of Pd toward ethanol electrooxidation, bimetallic Pd/M (M = Ru, Au, Ir, Sn, Ni) catalysts have been intensively studied in alkaline media.[5-8] Another possibility to enhance the performances of Pd based catalyst is the use of a catalyst support with a high surface area and a better stability than conventional carbon black.[3] The catalyst substrate should promote the formation of well-dispersed and stable Pd particles. The support, in addition to its structural role, can have an electronic effect on the catalyst phase and influence the catalytic activity of metallic particles via metal-support interaction (MSI).[9-11] This in turn will affect the adsorption strength of ethanol and reaction intermediates resulting in improved catalyst activity and in some cases its selectivity. Numerous nanostructured substrates such as carbon microspheres, hollow carbon spheres, nanowires and carbon nanotubes (CNTs) have been investigated to enhance the catalytic efficiency of Pd and to reduce the costs.[12-13] Nevertheless, carbon-based materials are not stable and corrode under reaction conditions. TiO_2 is well known for its high stability and its strong MSI with Pt group metals.[9] It is thus an interesting support for Pd particles.[14] Among the numerous types of titanium dioxide nanostructures, the nanotubes are interesting because the exhibit a high specific area and a well-defined geometry. TiO_2 nanotubes (TNTs) can be obtained by different methods such hydrothermal reaction, deposition in templates, molecular assembly templating, electrospinning and anodic oxidation.[15] The later method is straightforward and offers a large control of the tube morphology. In anodic TNTs, the charge transport and collection are

facilitated by the nanotubes self-alignment, because they are connected by the Ti substrate. In a previous work,[16] it has been shown that anodic TNT arrays can be suitable supports for Pd nanoparticles grown by atomic layer deposition (ALD) and that the annealing of titania improves the electrocatalytic activity of the catalysts. Although a high and stable electroactivity has been measured on such Pd/TNT systems further improvements are proposed in the present work through the addition of a SnO_2 interlayer between TNTs and Pd nanoparticles.

SnO_2 has been widely studied for application in sensors, batteries, photovoltaic cell, optoelectronic device and catalytic application.[17] There are a number of studies that show a promotional effect of SnO_2 support on alcohol electrooxidation.[18-21] A chemical modification of TNT surface by SnO_2 deposition is therefore suitable to enhance the Pd properties toward ethanol electrooxidation. Several techniques can be used to functionalize TNTs with SnO_2. The SnO_2 has been deposited onto anodic TNTs by solvothermal method,[22] by electrodeposition[23] or by ultrasonic deposition.[24] However, ALD remains a method of choice to grown conformal, particles[25] or continuous[26-27] oxide layers as well as sulphide[28-29] films and specially SnO_2 onto such nanostructures.[30-31] To avoid any film contamination, a process with non-halogenated precursor has been used.[30, 32] In recent years, many groups have reported the interest of using ALD to grow metallic nanoparticles onto nanostructured substrate.[33-36] The amount and the composition of the catalyst are fully controlled, the nanoparticles exhibit the same or better performances than particles grown by other methods.[16, 37-39]

The aim of the present study is to compare the electrochemical response of Pd catalysts supported by two different nanostructured materials: bare TNTs and SnO_2 coated TNTs. Since the SnO_2 deposition proceeds with a negligible variation of the geometry, the influence of the chemical nature of the substrate is solely expected. As schematically presented on Fig. 1, the SnO_2 layer and Pd nanoparticles have been successively deposited by ALD onto anodic TNTs (Pd/SnO_2/TNTs). The morphology, the chemical composition and the crystalline structure of the SnO_2 layer and the Pd catalysts have been investigated by scanning and transmission electron microscopies (SEM and TEM, respectively), x-ray photoelectron spectroscopy (XPS) and x-ray diffraction (XRD). The electroactivity of the Pd/SnO_2/TNTs systems toward ethanol electrooxidation has been measured by cyclic voltammetry (CV) and chronoamperometry (CA) as a function of the ALD parameters and depending on the crystalline structure of the SnO_2/TNTs support.

EXPERIMENTAL

Preparation of TiO_2 nanotubes

The TiO_2 nanotubes have been grown by anodization of Ti foils (Advent, 95.6% purity) in an aqueous fluoride containing acidic electrolyte (1 M H_3PO_4 + 1 M NaOH + 0.5% HF) as described in a previous publication.[40] The electrochemical oxidation was performed under a constant applied potential (U) of 20 V at room temperature using a high-voltage Modulab potentiostat (Solartron Analytical).

Atomic layer deposition of SnO_2

The SnO_2 layer was grown by atomic layer deposition in a Fiji 200 reactor from Ultratech/Cambridge Nanotech. The deposit was achieved at T = 200°C with tetrakis(dimethyl-amino)tin (TDMASn, 99.99%, from Strem chemicals) and hydrogen peroxide (30% from Sigma-Aldrich). In order to achieve a high growth per cycle (GPC) H_2O_2 has been chosen as oxygen source (*Caution: when performing the ALD process, the H_2O_2 concentration in the canister can increase due to a distillation phenomenon. The solution can become potentially explosive. A fresh solution should be used for each run*). The canister containing the TDMASn was held at T = 80°C. The so-called exposure mode was used to facilitate the deposition onto the whole TNTs. It consisted of isolating the reactor from the pumping system during each precursor pulse. The ALD process was therefore defined as the successive pulse, exposure and purge steps for both precursors. The sequence durations were 1:10:10 s and 1:10:10 s for TDMASn and H_2O_2, respectively. The ALD of SnO_2 was performed onto both TNTs and flat Si (100) substrates to facilitate some characterizations. The amount of deposited stannic oxide was controlled by the number of ALD cycles (N_{SnO_2}). Modification of the crystalline structure of SnO_2/TNTs was achieved by an annealing at 450°C for 2 h in air.

Atomic layer deposition of Pd

The deposition of the catalyst has been described previously.[41] It was carry out in the same reactor with palladium(II)hexafluoroacetylacetonate ($Pd(hfac)_2$, 98%, from Strem Chemicals) and formalin (37% formaldehyde in water with 10–15% of methanol from Sigma-Aldrich). The Pd canister was maintained at 90°C, while the temperature of the reaction chamber was set to 200°C.

The pulse, exposure, and purge durations were 1:30:30 s and 3:30:30 s for $Pd(hfac)_2$ and formalin, respectively. The number of ALD cycles (N_{Pd}) was varied to adjust the catalyst load.

Characterization Methods

The thickness of the SnO_2 deposit was measured by spectroscopic ellipsometry using a M2000V from J. A. Woollam Inc. The morphology of SnO_2/TNTs as well as the Pd/SnO_2/TNTs were characterized by SEM (JSM 6320F, JEOL) and TEM (JEM 3010, JEOL). The crystal structure of the SnO_2 layers and the TiO_2 substrates were analysed by XRD using a Rigaku RU-200 rotating anode x-ray generator (operating power 40 kV/30 mA) equipped with a Xenocs Fox3D Cu 12_INF mirror and a Mar345 image plate detector from Rayonix. Selected-area electron diffraction (SAED) was also performed in the TEM to locally study the crystal structure of the Pd/SnO_2/TNTs systems. The chemical composition of the deposits was determined by XPS using a Kratos Axis Ultra DLD with a Hybrid lens mode at 140 W and pass energy of 20 eV using a monochromatic Al K_α. The Sn 3d, Pd 3d and O 1s XPS core level spectra were analysed using a fitting routine which decomposes each spectrum into individual mixed Gaussian-Lorentzian peaks using a Shirley background subtraction over the energy range of the fit. The binding energy (BE) was corrected using the C 1s peak at 284.8 eV as an internal standard. The fitting of the Sn 3d was analysed using doublets with spin orbit splitting (SOS) 8.44 and intensity ratio Sn $3d_{5/2}$:Sn $3d_{3/2}$ = 3/2. The deconvolution of Pd 3d was performed using doublets with SOS 5.3 eV and intensity ratio Pd $3d_{5/2}$:Pd $3d_{3/2}$ = 3/2,[42] while a peak asymmetry was used in the case of the Pd 3d peak attributed to the metallic state based on the work of Hüfner et al.[43]

Electrochemical Characterizations

The electrochemical characterizations of Pd/SnO_2/TNTs were carried out in the conventional three-electrode electrochemical cell made of PTFE at room temperature. The BioLogic VSP potentiostat equipped with the EC-Lab software (BioLogic Science Instruments SAS) was used for electrochemical measurements in 1 M KOH with and without 1 M C_2H_5OH. The reference electrode used was a Hg/HgO (MMO, $E°$ = 0.098 vs SHE), and the counter electrode was a large surface area Pt mesh. Cyclic voltammetry was carried out at a scan rate of 25 mV s^{-1} unless otherwise stated. Chronoamperograms were performed by holding the potential at –0.6 V vs MMO

for 5 min and then stepping to –0.2 V for 1 h. All the potential are given versus the MMO reference electrode.

RESULTS

SnO_2 deposition onto TNTs

In order, to optimize the SnO_2 deposition different conditions have been investigated, such as the pulse and the purge durations as well as the reactor and the canister temperatures. The influence of those parameters on the growth rate has been studied and adjusted (Fig. S1). In the following, only the N_{SnO_2} was varied to control the thickness of SnO_2. SEM top views of TNTs with an increasing number of ALD cycles are shown on Figure 2 (N_{SnO_2} = 0, 20, 50, 100 and 150 cycles). The typical morphology of bare TNTs grown in an aqueous electrolyte is observed on Figure 2a. The diameter of the nanotubes is about 70 nm, the length is around 1 μm and the wall thickness is approximately 10 nm (additional SEM images are provided in Figure S2). After ALD of SnO_2, the wall thickness increases progressively with N_{SnO_2} (Figure 2b-e). For 150 ALD cycles the opening of some TNTs is even fully filled by the deposit. The thickness of the film (t_{SnO_2}) has been measured by spectroscopic ellipsometry on silicon wafers (Figure S1c). It reveals a linear increase of t_{SnO_2} with the number of ALD cycles. A GPC around 1.9 Å/cycle is then calculated from the slope of the straight evolution. This value is in line with the GPC reported previously by Elam et al.[31] The SEM images show a smooth and homogenous layer of SnO_2 onto the TNTs. They suggest a uniform coating of the TNTs but top views do not provide accurate information about the conformity. Thus, cross sectional observations have been performed by TEM.

The Figure 3 shows TEM cross-sections of TNTs after ALD of SnO_2 (N_{SnO_2} = 100 cycles). A large view presenting the tube mouth and walls is presented in Figure 3a where the TiO_2 appears as light grey while the SnO_2 film corresponds to the darker grey areas (for seek of clarity the SnO_2 layer is highlighted in blue). Although the opening of the voids located between the tubes is much smaller than the inner diameter, the ~~tin dioxide~~ SnO_2 deposition occurs similarly inside and outside the TNTs. The tubes are fully covered by a smooth and continuous layer of SnO_2. The thickness of the SnO_2 layer is rather constant on the different parts of the tube walls. As seen on Figure 3b, the deposition takes also place conformally at the bottom of the TNTs. The thickness of the SnO_2 layer

in the TNTs is approximately 16 nm. It is in agreement with the value (19 nm) obtained on plane Si.

The crystalline structure and the chemical composition have been investigated by XRD and XPS. The XRD patterns of as-grown and annealed SnO_2/TNT systems are compared on Figure 4. The diffractogram of the as-grown sample exhibits peaks from the Ti substrate (JCPDS #00-044-1294) and no crystalline TiO_2 is detected since the TNTs are usually amorphous after the anodization process. A small contribution from the rutile phase of SnO_2 (JCPDS #00-41-1445), also called cassiterite is also measured at 26.61°, 33.91° and 51.83° corresponding to the (110), (101) and (211) planes, respectively. After annealing at 450°C, two additional peaks ascribed to the plane (100) and (002) of the Ti appears at 35.00 and 38.45°, amorphous TiO_2 becomes crystalline. The peaks ascribed to the anatase structure (JCPDS #00-021-1271) are clearly visible at 25.33°, 48.08°, 53.93°, 55.12° and 62.75° which are attributed to the (101), (200), (105), (211) and (204) planes, respectively. After the thermal treatment, the diffraction peaks from SnO_2 are more intense and the presence of two additional peaks are visible at 37.92° and 39.00°. They correspond to the planes (200) and (111) of the cassiterite, respectively. The SnO_2 peaks are broad. They suggest a relatively small crystallite average size. As expected the survey spectrum of SnO_2/TNTs (shown in Figure S3) contains peaks corresponding to Sn, O and C.

The XPS spectrum of Sn 3d is presented in Fig 5a. The peaks centred at 487.1 and 495.5 eV are attributed to Sn $3d_{5/2}$ and Sn $3d_{3/2}$, respectively.[44-46] The deconvolution of the Sn 3d peaks reveals the existence of tin atoms in the oxidation state 4+, it can be deduced the presence of stoichiometric SnO_2. The spectrum of O 1s peak is shown on Figure 5b. It can be deconvoluted with two contributions. The main one, centred at 531 eV, is attributed to O^{2-} in SnO_2 and the other one positioned at 532.5 eV is ascribed to adsorbed oxygen or to the presence of water. This analysis confirms the high purity of the deposit and the absence of Ti peaks indicates a good coverage of TNT by ALD of SnO_2. In the following, 75 ALD cycles (i. e. approximately 14 nm) have systematically been used to grow SnO_2 on TNTs. The resulting SnO_2/TNTs were either used as-grown or after an annealing at T = 450°C.

Palladium deposition

The morphology of the Pd particles deposited onto as-grown SnO_2/TNTs has been observed by SEM. As shown in the previous part for ~~tin dioxide~~ SnO_2, ALD is commonly used to grow

continuous films. Though the SEM top view (Figure 6a) shows Pd nanoparticles uniformly spread onto the SnO_2/TNTs and not a continuous metallic film.

This phenomenon is expected since there is a high difference of surface energies between the metal and the oxide.[47] A similar island-growth mechanism has been observed for Pt deposited by ALD onto SnO_2 nanowires by Lin et al.[48] The deposition of Pd is homogenous along the outer wall of the SnO_2/TNTs (Fig 6b). It indicates the deposition of the nanoparticles proceeds within the narrow interstitial voids but these SEM observations give no evidence of Pd deposition inside the tubes. A similar morphology has been reported previously for direct ALD of Pd onto TNTs.[16] However when the TNTs are covered by the SnO_2 film, the geometry of the palladium catalysts appear more uniform.[8] It is well known that the nature of the substrate influences the ALD of metals. The ALD of Pd on ZnO and Al_2O_3 has, indeed, revealed that Pd grows faster on ZnO but a better uniformity is observed on Al_2O_3.[49] TEM observations have been performed to investigate the Pd deposition within the TNTs. Fig 7a shows a cross sectional view of a TiO_2 nanotube after successive depositions of SnO_2 and Pd (N_{SnO2} = 75 cycles and N_{Pd} = 500 cycles). Similarly to Figure 3, the SnO_2 layer appears in dark grey and coats the entire TNTs. Fig 7a demonstrates that the Pd particles uniformly cover the inner walls of the SnO_2/TNTs. The TEM top view (Figure 7b) confirms the presence of the nanoparticles on both sides of the tube walls. The high-resolution view (Figure 7c) reveals the atomic planes of the palladium catalysts and confirms therefore their crystalline structure. The SAED achieved on Pd deposited onto annealed SnO_2/TNTs is presented in Figure 7d. The pattern is composed by numerous spots and rings. The diffuse rings are attributed to a small amount of SnO_2, the presence of intense spots on the rings can be attributed to larger crystallite size. The other spots are attributed to the Pd and the anatase phase. The indexation of the different phases is presented in Figure S6. All the main diffraction planes are visible for the three phases and no preferential orientation is noticed.

It is well known that the growth of metallic particles can be affected by the chemical nature and the crystalline structure of the support.[50-51] The comparison of the ALD of Pd on bare and SnO_2-covered TNTs illustrates this effect. While an incubation delay (N_{Pd} = 400 cycles) is observed when depositing Pd on bare TNTs,[16] active particles are grown on SnO_2 for a lower number of ALD cycles since an electroactivity is measured for N_{Pd} = 100 cycles (see Figure 9). This can be explained by the action of the formaldehyde that reduces the SnO_2 during the second step of the ALD cycle. The XPS measurements that have been performed on Pd/SnO_2/TNTs before and after

electrochemical characterizations show indeed a modification of the chemical nature of the top surface (Figure 8). The analysis of the Sn $3d_{5/2}$ peak, shown in Figure 8c, indicates the reduction of the SnO_2 to metallic tin since contribution corresponding to the oxidation state 0 replaces the peak attributed to the oxidation state +4 (a detailed analysis of the XPS plots is given below). As the surface of the support is not an oxide but an ultrathin layer of metallic Sn, the nucleation of stable Pd is facilitated. A slight effect of the thermal treatment performed prior to ALD of Pd is also observed. After annealing, one observed the decrease of the particle diameter (e. g.: d_{Pd} varies from 10 to 6 nm for N_{Pd} = 600 cycles, see Figure S4) while the particle density (e. g.: n_{Pd} varies from 6.3 10^9 to 14.2 10^9 particles per cm^2 for N_{Pd} = 600 cycles) is increased. It suggests that the Pd nucleation proceed more easily on crystallized substrate.

XPS measurements were performed before and after the electrochemical measurements (EC), on annealed $Pd/SnO_2/TNTs$, in order to obtain a better insight into the surface chemical composition of the samples. The analysis of the survey (Figure 8a) shows that, in sample before electrochemical measurements, C, O, Sn and Pd were detected while no Ti was detected due to the attenuation of its signal from the overlayers. The carbon contribution may be attributed to surface contamination or residual carbon from the precursor.[52] Additionally the O 1s peak is overlapped by the Pd $3p_{3/2}$ making its interpretation rather not straightforward. The deconvoluted Pd 3d and Sn $3d_{5/2}$ before the EC are shown in Figure 8b and 8c. The analysis of the Pd $3d_{5/2}$ peak (Figure 8b) reveals the existence of two peaks at 335.5 and 337.5 eV. One, located at the lower binding energy, is attributed to palladium atoms in the metallic state while the one, at higher binding energy, is characteristic of Pd^{4+} in PdO_2.[53] The ratio of relative intensities of the two components Pd^0:Pd^{4+} is 93:7 showing that Pd is mainly in the metallic state. This is slightly different from the analysis of Pd particles grown on TNTs where only metallic Pd has been observed. On the other hand, the analysis of the Sn $3d_{5/2}$ XPS peak shows the existence of three components at 485.1, 486.1 and 487.2 eV attributed to Sn^0, Sn^{2+} and Sn^{4+}.[54-55] The relative intensities of the three components Sn^0:Sn^{2+}:Sn^{4+} are 75.0:12.4:12.6. The high amount of Sn^0 was not expected but it can be explained by deposition method of Pd. During the ALD of Pd, the formalin, a reductive precursor, can reduce the tin species at the surface from Sn^{4+} to Sn^0. This phenomenon is different from what has been previously observed on bare TNT surface.[16] As predicted by the Ellingham diagram,[56] it indicates that SnO_2 is less stable than TiO_2 toward the reduction by formalin. The metallic tin is essentially

localized at the top surface of the film, around 2 nm, which corresponds to the escape depth of the photoelectrons during the XPS experiments. The SAED performed on the Pd/SnO_2/TNTs have, however, confirmed that the bulk material is composed by SnO_2 (Figure 7d).

After the electrochemical measurements, the analysis of the survey (Figure 8a´) shows that C, Sn and Pd are still detected but the intensities are notably lower. After the EC, a significant amount of potassium is detected on the surface as indicated by the K 2p peak around 293.4 eV. The deconvolution of the Pd 3d peak (Figure 8b´) reveals that beyond the component at lower BEs (Pd $3d_{5/2}$: 335.1 eV) due to metallic Pd, two additional peaks are present at higher BEs (336 and 337.1 eV). These two peaks are attributed to palladium in the 2+ and 4+ oxidation states related to PdO and PdO_2 and/or hydroxides.[57-58] The relative intensities of the three components Pd:Pd^{2+}:Pd^{4+} is now 39.8:41.1:19.1. It is therefore evident that after the electrochemical measurements, oxidation of palladium has taken place as well and around 60% of the detected signal is due to oxygenated species. At this point we cannot exclude the formation of surface complexes that contains potassium as well, the K $2p_{3/2}$ is detected around 293.4 eV. In the literature, this binding energy is reported for potassium atoms in ionic compounds and K/Pd.[47] It is also well-known that all alkali metals, including potassium, form oxopalladates (K_nPdO_m).[59] The formation of this complex could explain the decrease of the signal from C, Sn and Pd. Further investigation is necessary to obtain a better insight of the K-based surface species. The analysis of the Sn $3d_{5/2}$ shows the existence of only one component at 487.2 eV, due to SnO_2.[54]

Electrocatalytic activity

Electrochemical response in KOH — Figure 9 shows cyclic voltammograms of Pd/SnO_2/TNT electrocatalysts and SnO_2/TNT support without Pd in 1 M KOH. The current density of the bare support is very low indicating, thus, no catalytic activity. The CVs of various Pd loads exhibit the characteristic peaks of Pd oxidation (ca. –0.2 V) and reduction (ca. –0.25 V). The region of hydrogen adsorption, absorption and desorption is visible at more negative potentials. The current density (per geometric area) rises with increasing the number of ALD cycles up to 500 cycles and then decreases because the coalescence of the Pd particles begins. It should be noted that in our previous work carried out on Pd/TNTs, neither oxidation nor reduction peaks of Pd were observed on CVs performed in 1 M KOH for NPd < 500 cycles.[16] Conversely, SnO_2-covered TNTs exhibit an electrochemical response for a Pd loading as low as 100 ALD cycles. This confirms that stable

Pd nuclei are formed on such substrate at low N_{Pd}. As mentioned above, this can be ascribed to the reduction of the SnO_2 to metallic tin at the top surface. The enhancement of the current response can also be attributed to the high electronic conductivity of SnO_2 (here 10^{-3}-10^{-2} Ω cm while Tighineanu et al.[60] have reported 10^{3}-10^{4} Ω cm for TNTs) that allows efficiently interconnect highly dispersed Pd nanoparticles and to MSI interaction between Pd and SnO_2.

Ethanol electrooxidation on Pd/SnO_2/TNT: effect of the annealing — In order to compare the intrinsic electrocatalytic activity of Pd/SnO_2/TNT samples, the current densities were normalized with respect to the electrochemical surface area (ECSA) that is estimated using PdO reduction peak in 0.5 M H_2SO_4, as reported previously.[16, 61] The ECSA was measured on as-grown and annealed SnO_2/TNTs with different Pd loads and the values are plotted in Figure S5. It is found that the ECSA increases with N_{Pd} and drops after reaching a maximum. Such evolution is measured for both as-grown and annealed samples but the active area is significantly lower after annealing. This is despite the lower particle size (ca. 2× lower) and the higher number of particles (ca. 2× higher), observed for all samples after annealing.[62] This trend is rather unusual, because one would expect the higher number of active surface atoms for the smaller particles in comparison to the larger ones. Furthermore, Sun et al. showed that the crystalline SnO_2, after annealing increased the ECSA if compared to amorphous SnO_2 in as-grown sample, however no morphological difference was found on Pt particles.[63] In the present case, the evolution of the ECSA seems to be solely related to geometric considerations. Thus the expansion of the ECSA with N_{Pd} can be attributed to the enlargement of the Pd particles (i. e. the rise of their geometric area) while the sudden decrease can be ascribed to their coalescence. The observed decrease of ECSA after annealing could be related to the interaction between SnO_2 and Pd nanoparticles leading to the partial coverage of Pd surface by oxygenated species from SnO_2. When Pd is supported on SnO_2 the electronic type MSI may raise at the interface of the two solids due to the charge transfer from the support to Pd (from the solid with lower work function (WF) to the solid with higher WF) and/or the higher availability of hydroxyl ions from SnO_2 that adsorb on the catalyst surface leading to lower ECSA, however these oxygenated species could have a promotional effect on ethanol electrooxidation.[53]

Figure 10 shows the CVs of as-grown and annealed SnO_2/TNT with 500 ALD cycles Pd in 1 M KOH + 1 M C_2H_5OH. The current density is higher for Pd deposited on the annealed support in the whole range of the anodic potential. The current density increases until it reaches a maximum at

0.251 and 0.275 V for as-grown and the annealed samples, respectively. The decrease of the current density is due to the surface palladium oxide formation,[64] which is not active for ethanol electrooxidation. On the reverse scan, the Pd activity is recovered at –0.19 and –0.24 V for as-grown and the annealed samples, respectively, due to PdO_x reduction to metallic Pd. The current density is much higher for Pd grown on annealed SnO_2/TNT and the onset potential is shifted negatively, –0.5 and –0.6 V for Pd deposited on as-grown and annealed supports, respectively. The increasing of the catalytic activity can be attributed to several factors: the increased conductivity of both oxides (SnO_2/TiO_2) after annealing and MSI effect.[62] Chen et al. have demonstrated an easier CO oxidation on crystalline Pt/SnO_2, suggesting a stronger interaction between Pt and crystalline SnO_2 than between Pt and amorphous SnO_2 support.[63] As shown previously,[16] the Pd particles deposited on annealed TNTs support exhibited a higher catalytic activity for ethanol electrooxidation reaction (as seen thereinafter, in Figure 13a, the maximum current ratio is higher than 4).

Ethanol electrooxidation on annealed Pd/SnO_2/TNT : effect of the Pd charge — Figure 11a shows the linear sweep voltammetry (LSV) of the annealed SnO_2/TNT with different amount of Pd (N_{Pd} = 300, 400, 500, 600, 800 cycles) in the ethanol containing electrolyte. The current density for ethanol electrooxidation increased with the number of ALD cycles up to 500 cycles and then the decrease occurred. This is illustrated in Figure 11b where the current density at –0.2 V is plotted against the N_{Pd}. This evolution indicates that from 300 to 500 ALD cycles the amount of available active sites for ethanol electrooxidation increases with the number of ALD cycles while at higher number of cycles, the increase of the particles size and the particle coalescence reduce the catalytic activity. Moreover, the MSI effect between Pd and SnO_2 may weaken as the particles become larger thus contributing to the decrease in the rate of electrooxidation.[65]

A similar behaviour was reported in a previous work, where the catalytic activity of 500 cycles of Pd deposited on TNTs was the highest. Chronoamperograms at –0.2 V for various loading of Pd interfaced with annealed SnO_2/TNT are presented on the Figure 12. The initial current density and the order of activities are in agreement with LSV results. For the samples with 300 and 800 cycles of Pd, the current density is low at the beginning 0.23 and 0.07 mA cm^{-2}, respectively. Then it decreases quickly until it reaches a steady-state at 0.16 and 0.05 mA cm^{-2}, respectively. For the samples with 400, 500, 600 cycles the current density is higher at the beginning 0.35, 0.40 and

0.27 mA cm^{-2}, respectively and continuously decreases without reaching a steady state after 1 h. The current percentage loss (without double layer correction) is 32, 50, 55, 45 and 34% for 300, 400, 500, 600 and 800 cycles of Pd, respectively. The current decrease is attributed to Pd oxide and oxopalladate formation as found from XPS analysis on the catalyst after electrochemical measurements (Fig. 8).

Ethanol electrooxidation: effect of the chemical nature and the crystalline structure of the support — Figure 13a compares the effect of the chemical nature of the support and the annealing for 500 cycles Pd/SnO_2/TNT catalyst. In order to compare the present results with literature, the Pd load (i. e., the mass of Pd, m_{Pd}, per area unit) has been estimated from the ECSA and the d_{Pd}. The LSVs of Pd deposited on as-grown TNTs, annealed TNTs, as-grown SnO_2/TNTs and annealed SnO_2/TNTs show that annealing and addition of SnO_2 interlayer enhance the ethanol electrooxidation. The positive effect of the support annealing has already been shown on bare TNTs[16] and is further confirmed in this work for SnO_2-covered TNTs. Since the morphology of the structured support is not significantly modified after the deposition of the thin SnO_2 layer (N_{SnO2} = 75 cycles), the evolution of the electrochemical response can not be attributed to geometric considerations. The LSVs of the as-grown TNTs and SnO_2/TNTs catalysts with 500 cycles Pd clearly show that addition of SnO_2 interlayer increases the current density of ethanol electrooxidation. The current density is significantly higher for Pd on SnO_2/TNTs than for Pd/TNTs and the onset potential is shifted negatively from –0.26 to –0.45 V for as-grown TNTs and SnO_2/TNTs, respectively.

This is in line with previous reports for Pt and Pd catalysts where SnO_2 showed strong contribution towards the improved catalytic activity of the metal.[66-67] For instance, Ruiz et al.[62] have shown that Pt-SnO_2-C has higher activity for methanol electrooxidation as compared to Pt-TiO_2-C. The high catalytic activity was attributed to the smaller Pt particle size obtained on SnO_2-C support. Moreover, Kim et al. have proposed a mechanism in which SnO_2 facilitates the oxidative removal of the intermediates residues on Pt for alcohol electrooxidation.[68] The addition of Sn species on Pt modifies its electronic environment by influencing the electron affinities of the surface Pt atoms and produces surface oxygenated species which can act as an oxidant source, thereby increasing stability through efficient oxidation of surface poisoning species. An et al. have reported that the catalytic activity of Pd has been enhanced by SnO_2 addition on TiO_2–MWCT for ethanol and

methanol electrooxidation.[20] This improvement is due to better particles dispersion and improvement of the resistance level to CO poisoning for methanol electrooxidation due to the increase of the concentration of OH_{ads} species on the Pd surface, which promotes the oxidation of acetaldehyde thus releasing active sites for the reaction.[22]

This effect is also visible by comparing annealed SnO_2/TNTs with annealed TNTs. The current density is further increased for annealed SnO_2/TNT support. Furthermore, Figure 13b shows a comparison of the current density obtained for 500 cycles of Pd on different supports at –0.2 V. As can be seen, the highest current density is obtained for annealed SnO_2/TNT with 500 cycles of Pd due to the increased conductivity of both oxides (SnO_2/TiO_2) after annealing, and to the metal-support interaction between Pd and SnO_2. The size of Pd clusters is smaller when grown on annealed SnO_2 (for $N_{Pd} \approx 600$ cycles, $d_{Pd} \approx 10$ nm and $d_{Pd} \approx 6$ nm for as-grown and annealed SnO_2/TiO_2, respectively). The smaller Pd particles may result in the stronger MSI effect. The MSI effect occurs at the interface of the two solids with different work function (WF): 5.2-5.6 and 4.6 eV for Pd and SnO_2, respectively.[69] The difference in WF will result in the charge transfer from the solid with lower WF to the solid with the higher one. The modification of electronic properties of Pd due to the charge transfer from the support and higher availability of oxygenated species or hydroxyl ions (OH^-) from SnO_2 to Pd, results in the higher catalytic activity of Pd/SnO_2/TNT.

Figure 14 compares of the activity of the best result of the present study (i. e. Pd/SnO_2/TNTs, $N_{Pd} = 500$ cycles after annealing) with similar systems reported in literature. The Pd particles are grown by various methods (electrochemical deposition, electrochemical deposition and milling, chemical deposition or ALD) on TNTs, carbon black, or multiwall CNTs. In some cases, the substrates are covered by SnO_2. Note that the experimental conditions (i. e. electrolyte composition and scanning rate, see Figure S7) are not exactly identical in all cases but sufficiently closed to be compared. Although the conditions are not advantageous for the present study, the measured activity is very closed to the best reported in literature.[70] The current density as well as the potential of the forward peak are better than on bare TNTs.[16] The comparison also suggests that SnO_2 seems to be a more efficient substrate to promote the electroactivity of Pd nanoparticles toward ethanol oxidation.

CONCLUSION

In this work, it has been shown that ALD was successfully used to functionalize TNTs with SnO_2 layer and Pd nanoparticles for ethanol electrooxidation. The depositions of both SnO_2 and Pd, are fully controlled and perfectly conformal onto the TNTs. The ALD of Pd on SnO_2-covered TNTs is facilitated because the top surface is reduced to metallic tin during the deposition of the particles. This synthesis method allows comparing the catalytic activity of Pd nanoparticles toward ethanol electrooxidation on different supports with no significant modification of the three-dimensional geometry. First, the modification of the chemical nature of the support has been investigated by the ALD of SnO_2 as an interlayer in between TNTs and Pd. The comparison between SnO_2 and TiO_2 surface has revealed that the SnO_2 has a promotional effect on Pd catalytic activity for ethanol electrooxidation. The positive impact of the addition of Sn species on Pd catalyst is well known and it is confirmed in this study. This fact can be attributed to several effects (i) the SnO_2 layer can facilitate the OH adsorption, (ii) the SnO_2 extreme surface is reduced to metallic Sn during ALD of Pd which favour the Pd growth and thereby the adsorption and the oxidation of ethanol are accelerated and (iii) MSI between Pd and SnO_2. Second, the influence of the crystalline structure of the support has been studied. The annealing of the support improves the electrocatalytic properties of Pd. According to this result the promoting effect can be attributed to several aspects: (i) the increased conductivity of the support by the annealing and (ii) MSI effect. The effect of the charge of Pd had also been investigated by varying the number of Pd ALD cycles. The best catalytic activity has been obtained for 500 ALD cycles on annealed SnO_2/TNTs. The electrochemical characterizations on such Pd/SnO_2/TNTs systems have evidenced a high current density and low onset potential compared to literature and commercial catalyst. In future studies, it would be interesting to investigate the catalytic properties of Pd deposited on SnO_2 nanotubes without TiO_2 and to investigate the potential effect of the deposition of a thin protective layer to stabilize the Pd activity for long term use. A recent study has shown that ALD of SnO_2 can be used on nanoparticles to enhance Pt catalytic durability for fuel cell application.[71]

ACKNOWLEDGEMENTS

The authors acknowledge V. Heresanu (CINaM) for XRD measurements, D. Chaudanson and S. Nitsche (CINaM) for their valuable help with the electron microscopy. A. Baronnet (CINaM) is also acknowledged for fruitful discussions. R. Sinha Roy and Y Magnin are acknowledged (CINaM) for helping in graphics editing. This collaborative work was supported by the France-Canada Research Fund. M. K. S. Barr and L. Assaud are indebted to the Conseil Régional Provence-Alpes-Côte d'Azur and the CNRS for the PhD grants.

ASSOCIATED CONTENT

Supporting Information. Influence of ALD parameter on the growth of SnO_2 thin layer. SEM pictures of bare TiO_2 nanotubes. XPS survey TNTs after ALD of SnO_2. Morphology of Pd nanoparticles grown onto SnO_2-covered TiO_2 nanotubes. Evolution of the ECSA with N_{Pd}. SAED indexation of SnO_2/TNTs annealed after ALD of Pd. Experimental conditions of the CVs from which the forward ethanol electrooxidation peak current and potential are extracted. This material is available free of charge via the Internet at http://pubs.acs.org.

AUTHOR INFORMATION

Corresponding Authors

*To whom correspondence should be addressed: elena.baranova@uottawa.ca;

lionel.santinacci@univ-amu.fr

REFERENCES

(1) Rousseau, S.; Coutanceau, C.; Lamy, C.; Leger, J. M., Direct Ethanol Fuel Cell (DEFC): Electrical Performances and Reaction Products Distribution under Operating Conditions with Different Platinum-Based Anodes. *J. Power Sources* **2006**, *158*, 18-24.

(2) Antolini, E., Catalysts for Direct Ethanol Fuel Cells. *J. Power Sources* **2007**, *170*, 1-12.

(3) Bianchini, C.; Shen, P. K., Palladium-Based Electrocatalysts for Alcohol Oxidation in Half Cells and in Direct Alcohol Fuel Cells. *Chem. Rev.* **2009**, *109*, 4183-4206.

(4) Antolini, E.; Gonzalez, E. R., Alkaline Direct Alcohol Fuel Cells. *J. Power Sources* **2010**, *195*, 3431-3450.

(5) Bambagioni, V.; Bianchini, C.; Marchionni, A.; Filippi, J.; Vizza, F.; Teddy, J.; Serp, P.; Zhiani, M., Pd and Pt-Ru Anode Electrocatalysts Supported on Multi-Walled Carbon Nanotubes and Their Use in Passive and Active Direct Alcohol Fuel Cells with an Anion-Exchange Membrane (Alcohol = Methanol, Ethanol, Glycerol). *J. Power Sources* **2009**, *190*, 241-251.

(6) Feng, Y.-Y.; Liu, Z.-H.; Xu, Y.; Wang, P.; Wang, W.-H.; Kong, D.-S., Highly Active PdAu Alloy Catalysts for Ethanol Electro-Oxidation. *J. Power Sources* **2013**, *232*, 99-105.

(7) Monyoncho, E. A.; Ntais, S.; Soares, F.; Woo, T. K.; Baranova, E. A., Synergetic Effect of Palladium–Ruthenium Nanostructures for Ethanol Electrooxidation in Alkaline Media. *J. Power Sources* **2015**, *287*, 139-149.

(8) Neto, A. O.; da Silva, S. G.; Buzzo, G. S.; de Souza, R. F. B.; Assumpção, M. H. M. T.; Spinacé, E. V.; Silva, J. C. M., Ethanol Electrooxidation on PdIr/C Electrocatalysts In Alkaline Media: Electrochemical and Fuel Cell Studies. *Ionics* **2015**, *21*, 87-495.

(9) Tauster, S. J.; Fung, S. C.; Garten, R. L., Strong Metal-Support Interactions - Group-8 Noble-Metals Supported on TiO_2. *J. Am. Chem. Soc.* **1978**, *100*, 170-175.

(10) Hepel, M.; Kumarihamy, I.; Zhong, C. J., Nanoporous TiO_2-Supported Bimetallic Catalysts for Methanol Oxidation in Acidic Media. *Electrochem. Commun.* **2006**, *8*, 1439-1444.

(11) Ntais, S.; Isaifan, R. J.; Baranova, E. A., An X-Ray Photoelectron Spectroscopy Study of Platinum Nanoparticles on Yttria-Stabilized Zirconia Ionic Support: Insight into Metal Support Interaction. *Mater. Chem. Phys.* **2014**, *148*, 673-679.

(12) Xu, C. W.; Liu, Y. L.; Yuan, D. S., Pt and Pd Supported on Carbon Microspheres for Alcohol Electrooxidation in Alkaline Media. *Int. J. Hydrogen Energy* **2007**, *2*, 674-680.

(13) Zheng, H. T.; Li, Y. L.; Chen, S. X.; Shen, P. K., Effect of Support on the Activity of Pd Electrocatalyst for Ethanol Oxidation. *J. Power Sources* **2006**, *163*, 371-375.

(14) Huang, S. Y.; Ganesan, P.; Park, S.; Popov, B. N., Development of a Titanium Dioxide-Supported Platinum Catalyst with Ultrahigh Stability for Polymer Electrolyte Membrane Fuel Cell Applications. *J. Am. Chem. Soc.* **2009**, *131*, 13898-13899.

(15) Lee, K.; Mazare, A.; Schmuki, P., One-Dimensional Titanium Dioxide Nanomaterials: Nanotubes. *Chem. Rev.* **2014**, *114*, 9385-9454.

(16) Assaud, L.; Brazeau, N.; Barr, M. K. S.; Hanbucken, M.; Ntais, S.; Baranova, E. A.; Santinacci, L., Atomic Layer Deposition of Pd Nanoparticles on TiO_2 nanotubes for Ethanol Electrooxidation: Synthesis and Electrochemical Properties *ACS Appl. Mater. Interfaces* **2015**, *7*, 24533-24542.

(17) Batzill, M.; Diebold, U., The Surface and Materials Science of Tin Oxide. *Prog. Surf. Sci.* **2005**, *79*, 47-154.

(18) Wen, Z.; Yang, S.; Liang, Y.; He, W.; Tong, H.; Hao, L.; Zhang, X.; Song, Q., The Improved Electrocatalytic Activity of Palladium/Graphene Nanosheets Towards Ethanol Oxidation by Tin Oxide. *Electrochim. Acta* **2010**, *56*, 139-144.

(19) Lu, H.; Fan, Y.; Huang, P.; Xu, D., SnO_2 Nanospheres Supported Pd Catalyst with Enhanced Performance for Formic Acid Oxidation. *J. Power Sources* **2012**, *215*, 48-52.

(20) An, H.; Pan, L.; Cui, H.; Li, B.; Zhou, D.; Zhai, J.; Li, Q., Synthesis and Performance of Palladium-Based Catalysts for Methanol and Ethanol Oxidation in Alkaline Fuel Cells. *Electrochim. Acta* **2013**, *102*, 79-87.

(21) An, H.; Pan, L.; Cui, H.; Li, Q.; Zhai, J., Electrocatalytic Performance of Pd/SnO_2-TiO_2/MWCNT Catalyst for Oxidation of Ethylene Glycol in Alkaline Media. *J. Electrochem. Soc.* **2014**, *162*, F123-F128.

(22) Du, G.; Guo, Z.; Zhang, P.; Li, Y.; Chen, M.; Wexler, D.; Liu, H., SnO_2 Nanocrystals on Self-Organized TiO_2 Nanotube Array as Three-Dimensional Electrode for Lithium Ion Microbatteries. *J. Mater. Chem.* **2010**, *20*, 5689-5694.

(23) Wu, X.; Zhang, S.; Wang, L.; Du, Z.; Fang, H.; Ling, Y.; Huang, Z., Coaxial SnO_2@TiO_2 Nanotube Hybrids: from Robust Assembly Strategies to Potential Application in Li^+ Storage. *J. Mater. Chem.* **2012**, *22*, 11151-11158.

(24) Hu, J.; Liu, Q.; Zhang, H.; Chen, C.-D.; Liang, Y.; Du, R.-G.; Lin, C.-J., Facile Ultrasonic Deposition of SnO_2 Nanoparticles on TiO_2 Nanotube Films for Enhanced Photoelectrochemical Performances. *J. Mater. Chem. A* **2015**, *3*, 22605-22613.

(25) Turkevych, I.; Kosar, S.; Pihosh, Y.; Mawatari, K.; Kitamori, T.; Ye, J.; Shimamura, K., Synergistic Effect between TiO_2 and Ubiquitous Metal Oxides on Photocatalytic Activity of Composite Nanostructures. *J. Ceram. Soc. Jpn.* **2014**, *122*, 393-397.

(26) Jere, T.; Marianna, K.; Emma, H.; Mikko, R.; Markku, L., Preparation of regularly structured nanotubular TiO_2 thin films on ITO and their modification with thin ALD-grown layers. *Nanotechnology* **2012**, *23*, 125707.

(27) Zazpe, R.; Kraut, M.; Sopha, H.; Hromadko, L.; Albert, M.; Prikryl, J.; Gartnerova, V.; Bartha, J. W.; Macak, J. M., Atomic Layer Deposition for Coating of High Aspect Ratio TiO_2 Nanotube Layers. *Langmuir* **2016**, *32*, 10551-10558.

(28) Sarkar, S. K.; Kim, J. Y.; Goldstein, D. N.; Neale, N. R.; Zhu, K.; Elliott, C. M.; Frank, A. J.; George, S. M., In_2S_3 Atomic Layer Deposition and Its Application as a Sensitizer on TiO_2 Nanotube Arrays for Solar Energy Conversion. *J. Phys. Chem. C* **2010**, *114*, 8032-8039.

(29) Macak, J. M.; Prikryl, J.; Sopha, H.; Strizik, L., Antireflection ln_2O_3 Coatings of Self-Organized TiO_2 Nanotube Layers Prepared by Atomic Layer Deposition. *Phys. Status Solidi RRL* **2015**, *9*, 516-520.

(30) Elam, J. W.; Baker, D. A.; Martinson, A. B. F.; Pellin, M. J.; Hupp, J. T., Atomic Layer Deposition of Indium Tin Oxide Thin Films Using Nonhalogenated Precursors. *J. Phys. Chem. C* **2008**, *112*, 1938-1945.

(31) Elam, J. W.; Baker, D. A.; Hryn, A. J.; Martinson, A. B. F.; Pellin, M. J.; Hupp, J. T., Atomic Layer Deposition of Tin Oxide Films Using Tetrakis(Dimethylamino) Tin. *J. Vac. Sci. Technol. A* **2008**, *26*, 244-252.

(32) Mullings, M. N.; Hägglund, C.; Bent, S. F., Tin Oxide Atomic Layer Deposition from Tetrakis(Dimethylamino)Tin and Water. *J. Vac. Sci. Technol. A* **2013**, *31*, 061503.

(33) Detavernier, C.; Dendooven, J.; Pulinthanathu Sree, S.; Ludwig, K. F.; Martens, J. A., Tailoring Nanoporous Materials by Atomic Layer Deposition. *Chem. Soc. Rev.* **2011**, *40*, 5242-5253.

(34) Elam, J. W.; Dasgupta, N. P.; Prinz, F. B., ALD for Clean Energy Conversion, Utilization, and Storage. *MRS Bulletin* **2011**, *36*, 899-906.

(35) Weber, M. J.; Mackus, A. J. M.; Verheijen, M. A.; van der Marel, C.; Kessels, W. M. M., Supported Core/Shell Bimetallic Nanoparticles Synthesis by Atomic Layer Deposition. *Chem. Mater.* **2012**, *24*, 2973-2977.

(36) Lu, J.; Elam, J. W.; Stair, P. C., Synthesis and Stabilization of Supported Metal Catalysts by Atomic Layer Deposition. *Acc. Chem. Res.* **2013**, *46*, 1806-1815.

(37) Goldstein, D. N.; George, S. M., Enhancing the Nucleation of Palladium Atomic Layer Deposition on Al_2O_3 Using Trimethylaluminum to Prevent Surface Poisoning by Reaction Products. *Appl. Phys. Lett.* **2009**, *95*, 143106.

(38) Feng, H.; Libera, J. A.; Stair, P. C.; Miller, J. T.; Elam, J. W., Subnanometer Palladium Particles Synthesized by Atomic Layer Deposition. *ACS Catal.* **2011**, *1*, 665-673.

(39) Lu, J.; Liu, B.; Greeley, J. P.; Feng, Z.; Libera, J. A.; Lei, Y.; Bedzyk, M. J.; Stair, P. C.; Elam, J. W., Porous Alumina Protective Coatings on Palladium Nanoparticles by Self-Poisoned Atomic Layer Deposition. *Chem. Mater.* **2012**, *24*, 2047-2055.

(40) Assaud, L.; Heresanu, V.; Hanbuecken, M.; Santinacci, L., Fabrication of p/n Heterojunctions by Electrochemical Deposition of Cu_2O onto TiO_2 Nanotubes. *C. R. Chim.* **2013**, *16*, 89-95.

(41) Assaud, L.; Monyoncho, E.; Pitzschel, K.; Allagui, A.; Petit, M.; Hanbucken, M.; Baranova, E. A.; Santinacci, L., 3D-Nanoarchitectured Pd/Ni Catalysts Prepared by Atomic Layer Deposition for The Electrooxidation of Formic Acid. *Beilstein J. Nanotechnol.* **2014**, *5*, 162-172.

(42) Richter, K.; Peplinski, B., Energy Calibration of Electron Spectrometers. *J. Electron. Spectrosc. Relat. Phenom.* **1978**, *13*, 69-71.

(43) Hüfner, S.; Wertheim, G. K., Core-Line Asymmetries in the X-Ray-Photoemission Spectra of Metals. *Phys. Rev. B* **1975**, *11*, 678-683.

(44) Meng, X.; Yao, J.; Liu, F.; He, H.; Zhou, M.; Xiao, P.; Zhang, Y., Preparation of SnO_2@C-Doping TiO_2 Nanotube Arrays and Its Electrochemical and Photoelectrochemical Properties. *J. Alloys Compd.* **2013**, *552*, 392-397.

(45) Tian, Q.; Zhang, Z.; Yang, L.; Hirano, S., Encapsulation of SnO_2 Nanoparticles into Hollow TiO_2 Nanowires as High Performance Anode Materials for Lithium Ion Batteries. *J. Power Sources* **2014**, *253*, 9-16.

(46) Liao, J.-Y.; Manthiram, A., Mesoporous TiO_2-Sn/C Core-Shell Nanowire Arrays as High-Performance 3D Anodes for Li-Ion Batteries. *Adv. Energy Mater.* **2014**, *4*, 1400403.

(47) Campbell, C. T., Ultrathin Metal Films and Particles on Oxide Surfaces: Structural, Electronic and Chemisorptive Properties. *Surf. Sci. Rep.* **1997**, *27*, 1-111.

(48) Lin, Y.-H.; Hsueh, Y.-C.; Lee, P.-S.; Wang, C.-C.; Wu, J. M.; Perng, T.-P.; Shih, H. C., Fabrication of Tin Dioxide Nanowires with Ultrahigh Gas Sensitivity by Atomic Layer Deposition of Platinum. *J. Mater. Chem.* **2011**, *21*, 10552-10558.

(49) Feng, H.; Elam, J. W.; Libera, J. A.; Setthapun, W.; Stair, P. C., Palladium Catalysts Synthesized by Atomic Layer Deposition for Methanol Decomposition. *Chem. Mater.* **2010**, *22*, 3133-3142.

(50) Lei, Y.; Liu, B.; Lu, J.; Libera, J. A.; Greeley, J. P.; Elam, J. W., Effects of Chlorine in Titanium Oxide on Palladium Atomic Layer Deposition. *J. Phys. Chem. C* **2014**, *118*, 22611-22619.

(51) Mackus, A. J. M.; Matthieu, J. W., M. J.; Thissen, N. F. W.; Garcia-Alonso, D.; Vervuurt, R. H. J.; Assali, S.; Bol, A. A.; Verheijen, M. A.; Kessels, W. M. M., Atomic Layer

Deposition of Pd and Pt Nanoparticles for Catalysis: on The Mechanisms of Nanoparticle Formation. *Nanotechnology* **2016**, *27*, 034001.

(52) Gharachorlou, A.; Detwiler, M. D.; Nartova, A. V.; Lei, Y.; Lu, J.; Elam, J. W.; Delgass, W. N.; Ribeiro, F. H.; Zemlyanov, D. Y., Palladium Nanoparticle Formation on TiO_2(110) by Thermal Decomposition of Palladium(II) Hexafluoroacetylacetonate. *ACS Appl. Mater. Interfaces* **2014**, *6*, 14702-14711.

(53) Monyoncho, E. A.; Ntais, S.; Brazeau, N.; Wu, J.-J.; Sun, C.-L.; Baranova, E. A., Role of the Metal-Oxide Support in the Catalytic Activity of Pd Nanoparticles for Ethanol Electrooxidation in Alkaline Media. *ChemElectroChem* **2016**, *3*, 218-227.

(54) Briggs, D.; Seah, M. P., *Practical Surface Analysis by Auger and X-Ray Photoelectron Spectroscopy*; John Wiley and Sons Ltd: Chichester, 1996, p 674.

(55) Süzer, S.; Voscoboinikov, T.; Hallam, K. R.; Allen, G. C., Electron Spectroscopic Investigation of Sn Coatings on Glasses. *Fresenius J. Anal. Chem.* **1996**, *355*, 654-656.

(56) Howard, S. M., Ellingham Diagrams: Standard Gibbs Energies of Formation for Oxides. *SD School of Mines and Technology, Rapid City, SD* **2006**

(57) Shafeev, G. A.; Themlin, J. M.; Bellard, L.; Marine, W.; Cros, A., Enhanced Adherence of Area-Selective Electroless Metal Plating on Insulators. *J. Vac. Sci. Technol. A* **1996**, *14*, 319-326.

(58) Gao, W.; Jin, R.; Chen, J.; Guan, X.; Zeng, H.; Zhang, F.; Liu, Z.; Guan, N., Titania-Supported Pd–Cu Bimetallic Catalyst for the Reduction of Nitrite Ions in Drinking Water. *Catal. Lett.* **2003**, *91*, 25-30.

(59) Lee, H.-B.-R.; Bent, S. F., Microstructure-Dependent Nucleation in Atomic Layer Deposition of Pt on TiO_2. *Chem. Mater.* **2012**, *24*, 279-286.

(60) Tighineanu, A.; Ruff, T.; Albu, S.; Hahn, R.; Schmuki, P., Conductivity Of TiO_2 Nanotubes: Influence of Annealing Time And Temperature. *Chem. Phys. Lett.* **2010**, *494*, 260-263.

(61) Horkans, J., The Hydrogen Region of The Cyclic Voltammetry of Pd: The Effect of pH and Anion. *J. Electroanal. Chem.* **1986**, *209*, 371-376.

(62) Ruiz-Camacho, B.; Santoyo, H. H. R.; Medina-Flores, J. M.; Álvarez-Martínez, O., Platinum Deposited on TiO_2-C and SnO_2-C Composites for Methanol Oxidation and Oxygen Reduction. *Electrochim. Acta* **2014**, *120*, 344-349.

(63) Chen, Y.; Wang, J.; Meng, X.; Zhong, Y.; Li, R.; Sun, X.; Ye, S.; Knights, S., Pt–SnO_2/Nitrogen-Doped CNT Hybrid Catalysts for Proton-Exchange Membrane Fuel Cells (PEMFC): Effects of Crystalline and Amorphous Sno2 By Atomic Layer Deposition. *J. Power Sources* **2013**, *238*, 144-149.

(64) Liang, Z. X.; Zhao, T. S.; Xu, J. B.; Zhu, L. D., Mechanism Study of the Ethanol Oxidation Reaction on Palladium in Alkaline Media. *Electrochim. Acta* **2009**, *54*, 2203-2208.

(65) Wieckowski, A.; Savinova, E. R.; Vayenas, C. G., Particle Size, Support and Promotional Effects. In *Catalysis and Electrocatalysis at Nanoparticle Surfaces*, Marcel Dekker: New York, 2003; pp 613-847.

(66) Mao, H.; Wang, L.; Zhu, P.; Xu, Q.; Li, Q., Carbon-Supported PdSn–SnO_2 Catalyst for Ethanol Electro-Oxidation in Alkaline Media. *Int. J. Hydrogen Energy* **2014**, *39*, 17583-17588.

(67) Takabatake, Y.; Noda, Z.; Lyth, S. M.; Hayashi, A.; Sasaki, K., Cycle Durability of Metal Oxide Supports for PEFC Electrocatalysts. *Int. J. Hydrogen Energy* **2014**, *39*, 5074-5082.

(68) Kim, J. H.; Choi, S. M.; Nam, S. H.; Seo, M. H.; Choi, S. H.; Kim, W. B., Influence of Sn Content On PtSn/C Catalysts for Electrooxidation Of C1–C3 Alcohols: Synthesis, Characterization, and Electrocatalytic Activity. *Appl. Catal., B* **2008**, *82*, 89-102.

(69) Skriver, H. L.; Rosengaard, N. M., Ab Initio Work Function of Elemental Metals. *Phys. Rev. B* **1992**, *45*, 9410-9412.

(70) Chen, Y.-X., et al., Electrochemical Milling and Faceting: Size Reduction and Catalytic Activation of Palladium Nanoparticles. *Angew. Chem. Int. Ed.* **2012**, *51*, 8500-8504.

(71) Marichy, C.; Ercolano, G.; Caputo, G.; Willinger, M. G.; Jones, D.; Roziere, J.; Pinna, N.; Cavaliere, S., ALD SnO_2 Protective Decoration Enhances the Durability of a Pt Based Electrocatalyst. *J. Mater. Chem. A* **2016**, *4*, 969-975.

(72) Qin, Y.-H.; Yang, H.-H.; Lv, R.-L.; Wang, W.-G.; Wang, C.-W., TiO_2 Nanotube Arrays Supported Pd Nanoparticles forr Ethanol Electrooxidation in Alkaline Media. *Electrochim. Acta* **2013**, *106*, 372-377.

(73) Rikkinen, E.; Santasalo-Aarnio, A.; Airaksinen, S.; Borghei, M.; Viitanen, V.; Sainio, J.; Kauppinen, E. I.; Kallio, T.; Krause, A. O. I., Atomic Layer Deposition Preparation of Pd Nanoparticles on a Porous Carbon Support for Alcohol Oxidation. *J. Phys. Chem. C* **2011**, *115*, 23067-23073.

(74) Monyoncho, E. A.; Steinmann, S. N.; Michel, C.; Baranova, E. A.; Woo, T. K.; Sautet, P., Ethanol Electro-oxidation on Palladium Revisited Using Polarization Modulation Infrared Reflection Absorption Spectroscopy (PM-IRRAS) and Density Functional Theory (DFT): Why Is It Difficult To Break the C–C Bond? *ACS Catal.* **2016**, *6*, 4894-4906.

(75) An, H.; Cui, H.; Zhou, D.; Tao, D.; Li, B.; Zhai, J.; Li, Q., Synthesis and Performance of Pd/SnO_2-TiO_2/MWCNT Catalysts for Direct Formic Acid Fuel Cell Application. *Electrochim. Acta* **2013**, *92*, 176-182.

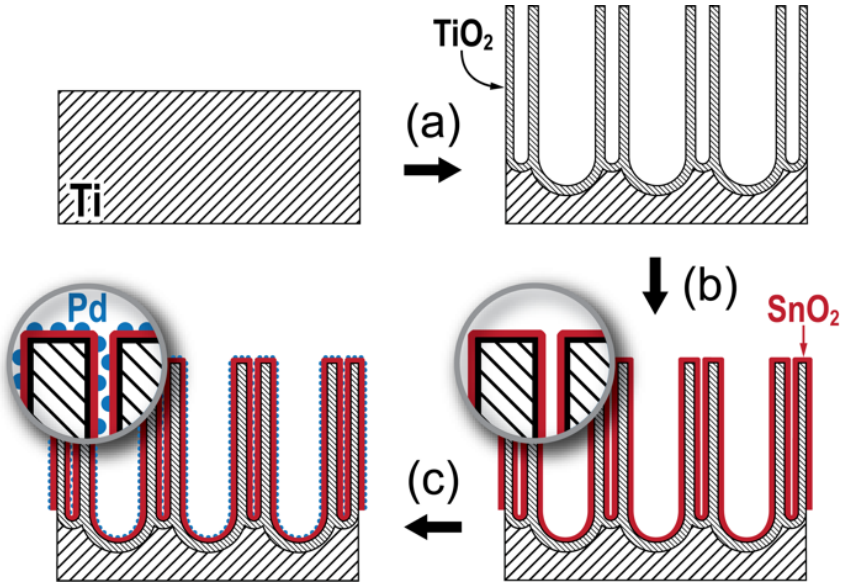

Figure 1: Schematic view of the process. (a) Anodic growth of the TiO_2 nanotubes, (b) ALD of SnO_2 and (c) ALD of Pd.

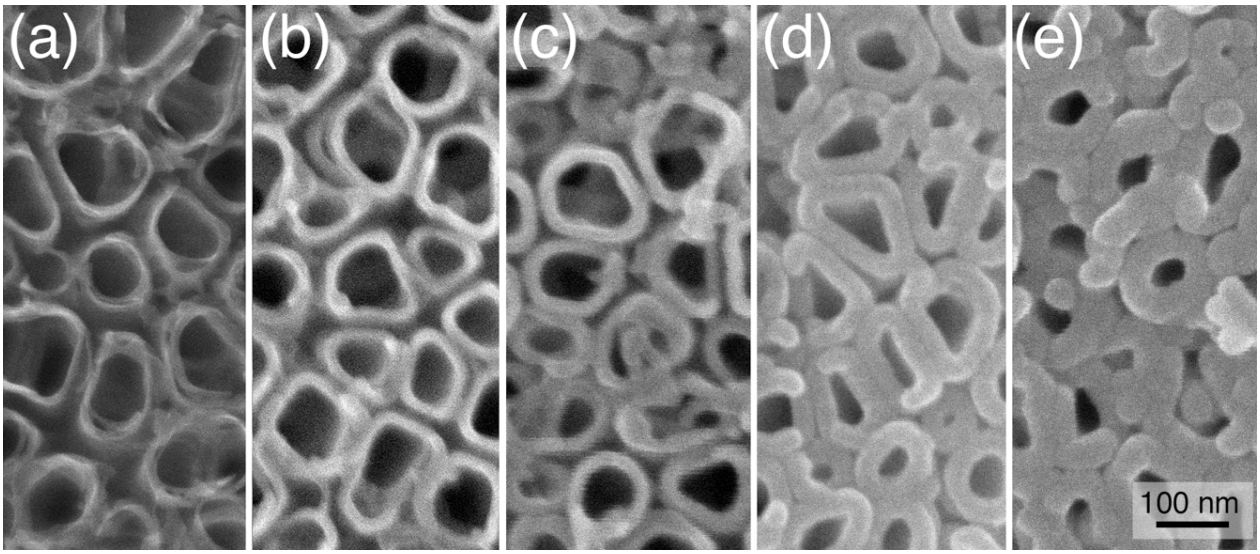

Figure 2: SEM top views of TiO_2 nanotubes covered by a thin SnO_2 layer. The number of ALD cycles (N_{SnO_2}) is increasing from 0 (a), 20 (b), 50 (c), 100 (d) to 150 cycles (e).

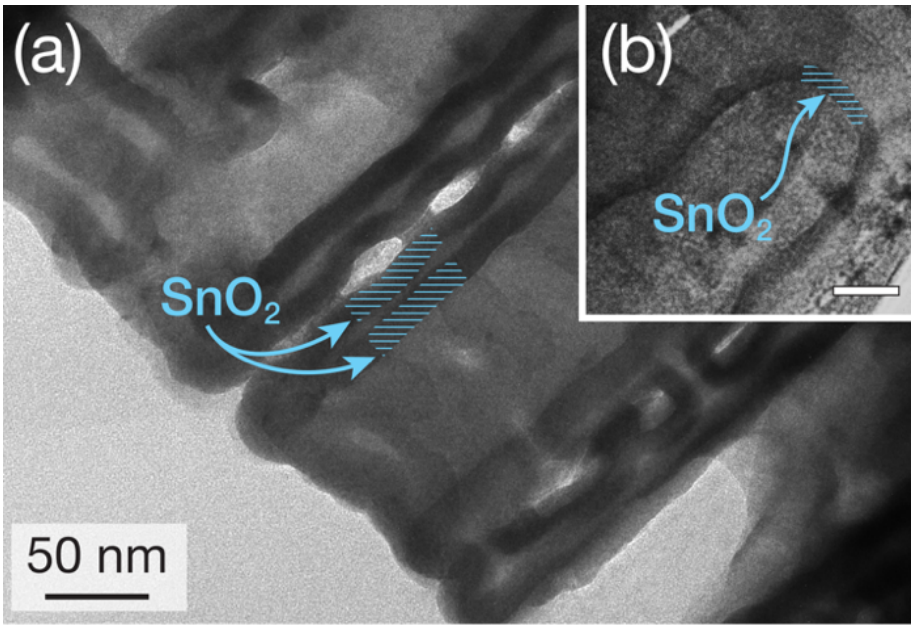

Figure 3: TEM cross sections of the opening (a) and the bottom (b) of TNTs after ALD of SnO_2 (a). The scale bar in (b) corresponds to 20 nm.

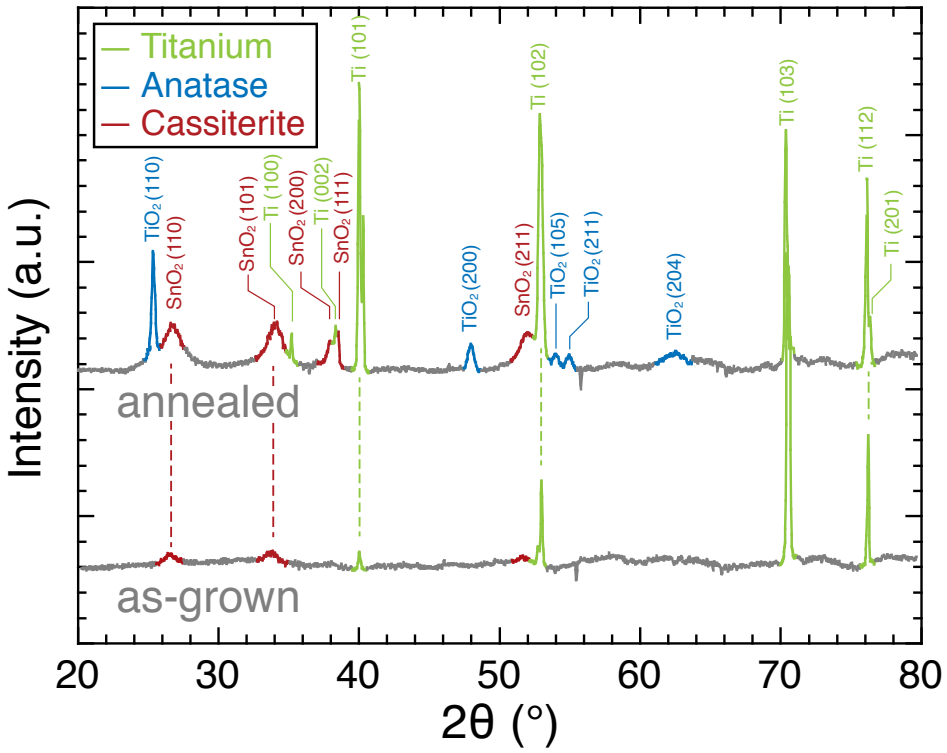

Figure 4: X-ray diffractograms of SnO_2-coated TNTs before (bottom) and after (top) annealing at 450°C

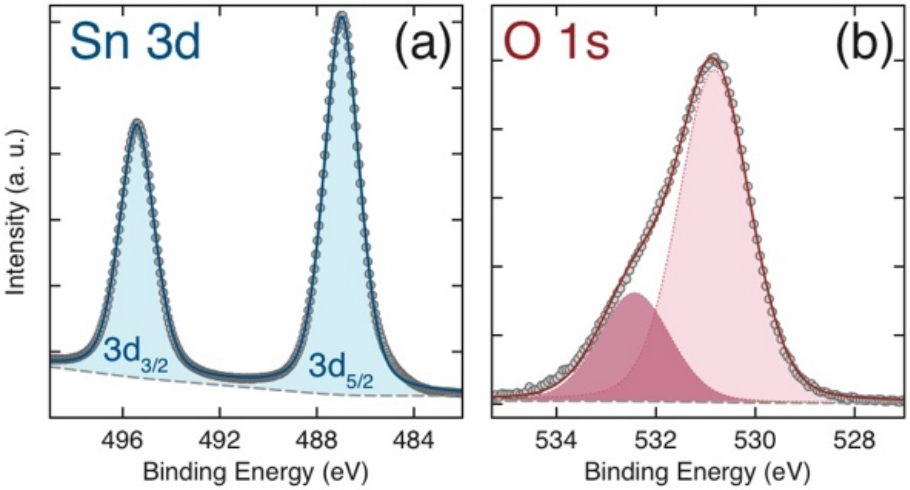

Figure 5: Sn 3d (a) and O 1s (b) XPS peaks of SnO_2-coated TNTs (N_{SnO_2} = 50 cycles)

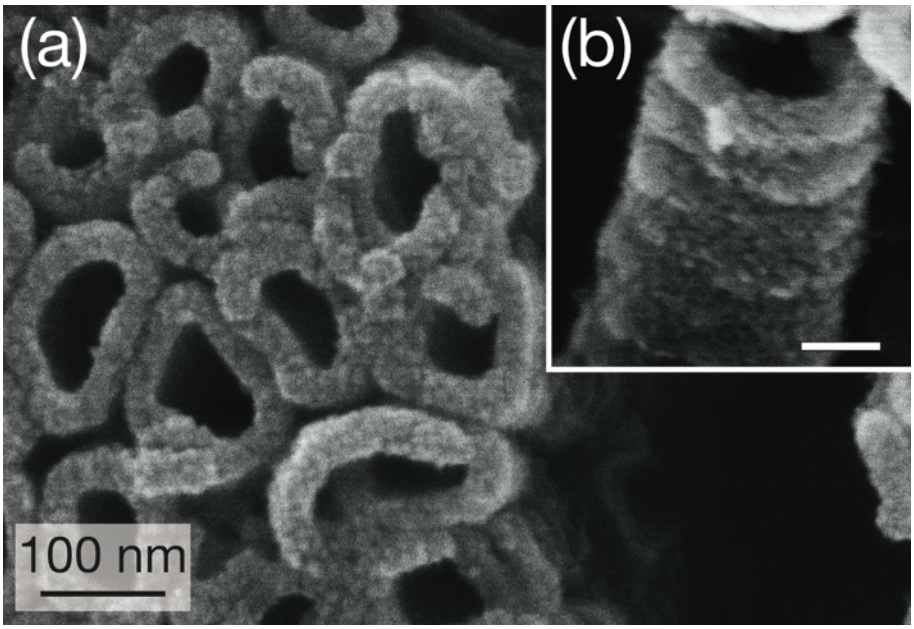

Figure 6: SEM images of SnO_2/TNTs after ALD of Pd (N_{Pd} = 600 cycles): (a) top view and (b) side view. The scale bar in (b) corresponds to 50 nm.

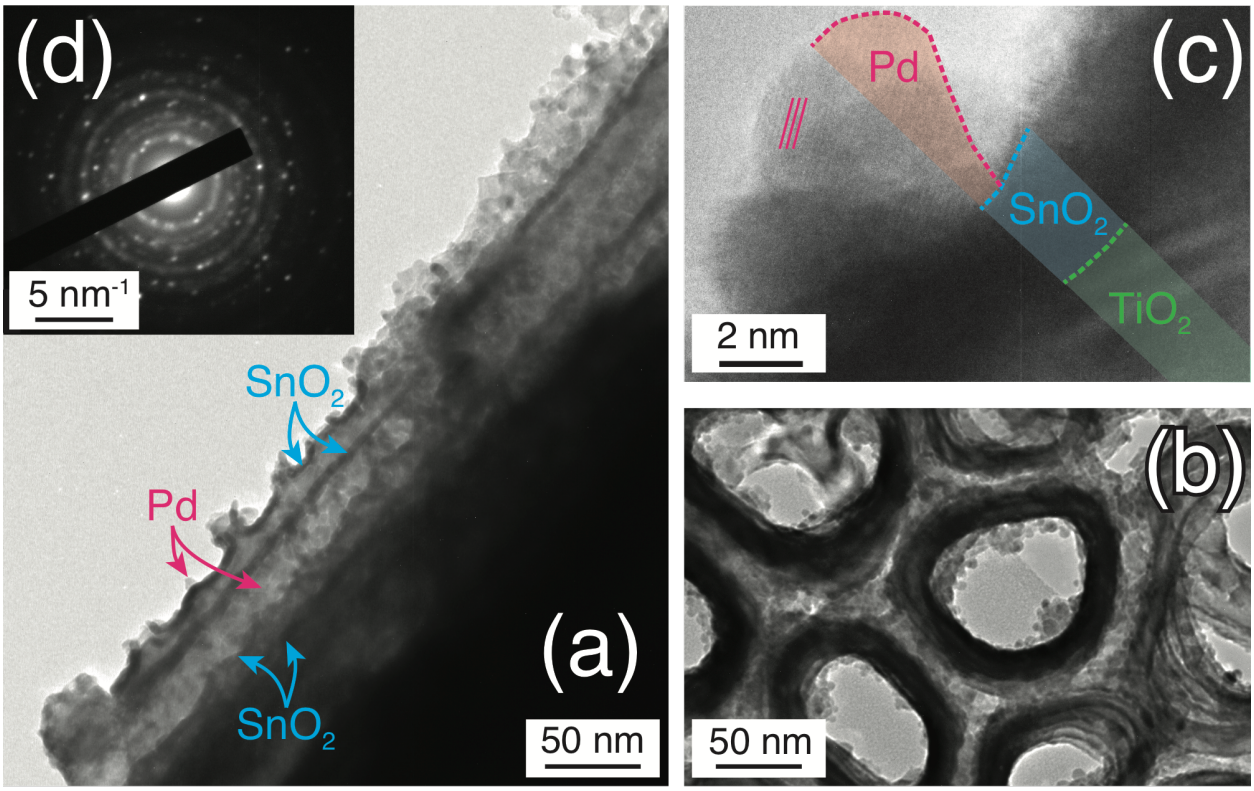

Figure 7: TEM images of SnO_2/TNTs annealed after ALD of Pd (N_{Pd} = 500 cycles): (a) cross section of a single nanotube, (b) top view of several nanotubes, (c) high-magnification of Pd particles on a tube wall and (d) SAED corresponding to the area shown in (b). The various materials are artificially colored in (c) for seek of clarity and the three red lines highlight the Pd crystal rows.

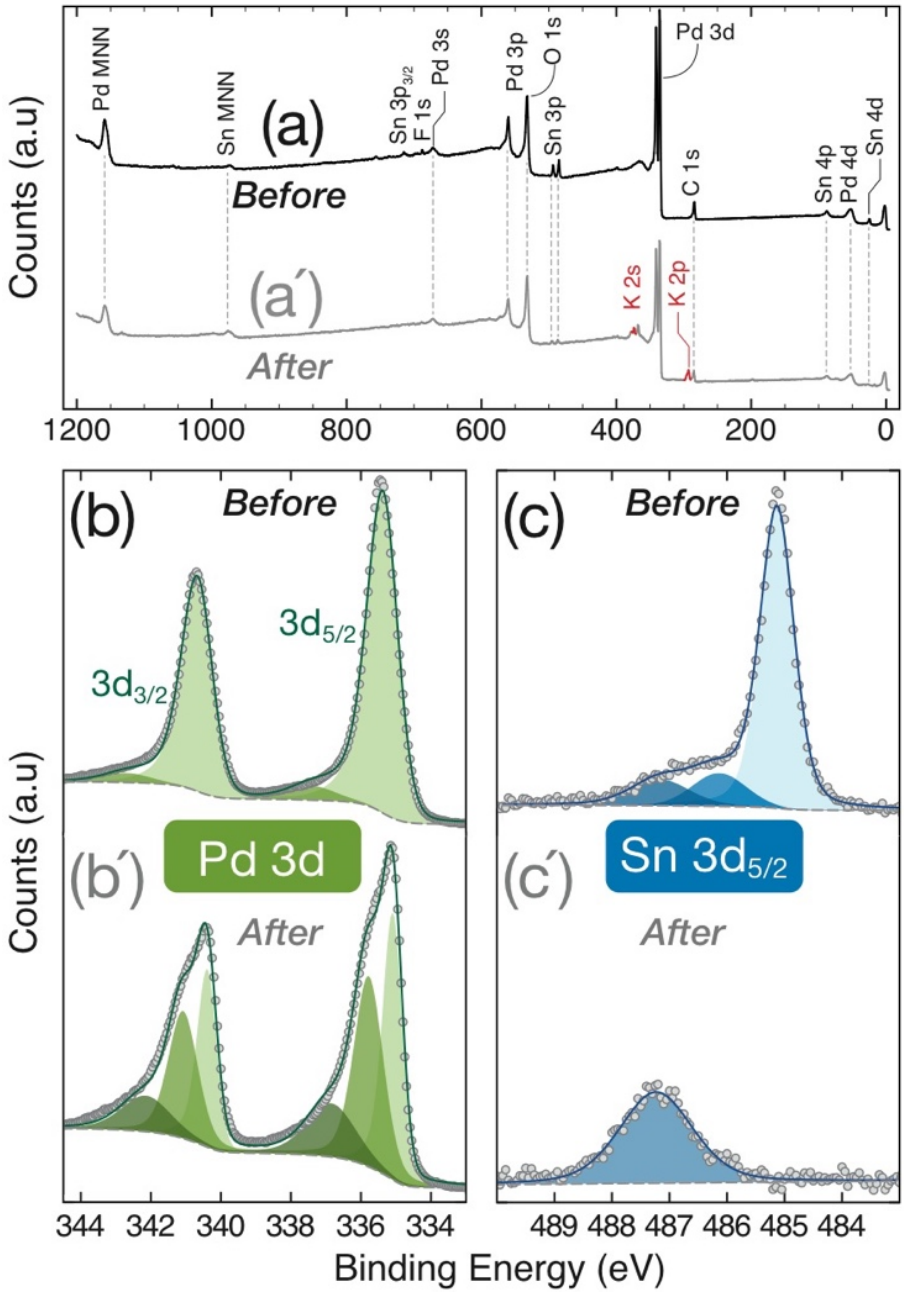

Figure 8: Comparison of the chemical composition of the surface before (a,b,c) and after (a´,b´,c´) electrochemical investigations performed on annealed Pd/SnO_2/TNTs. XPS survey (a,a´), Pd 3d peak (b,b´) and Sn 3d peak (c,c´).

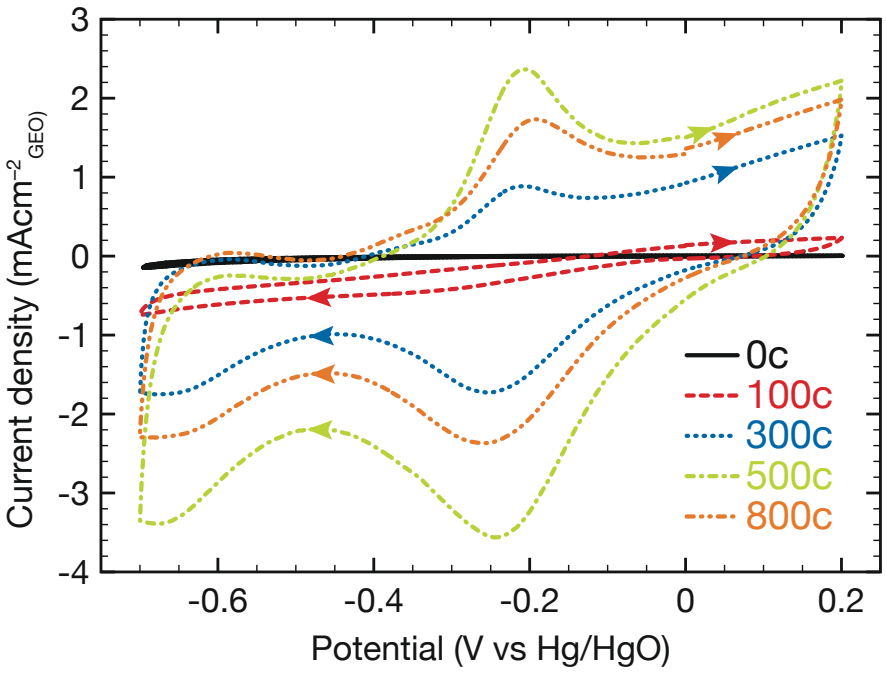

Figure 9: CVs of as-grown SnO_2/TNTs after ALD of Pd for N_{Pd}= 0, 100, 300, 500 and 800 cycles. The electrolyte is 1 M KOH and the scan rate is 25 mV s^{-1}.

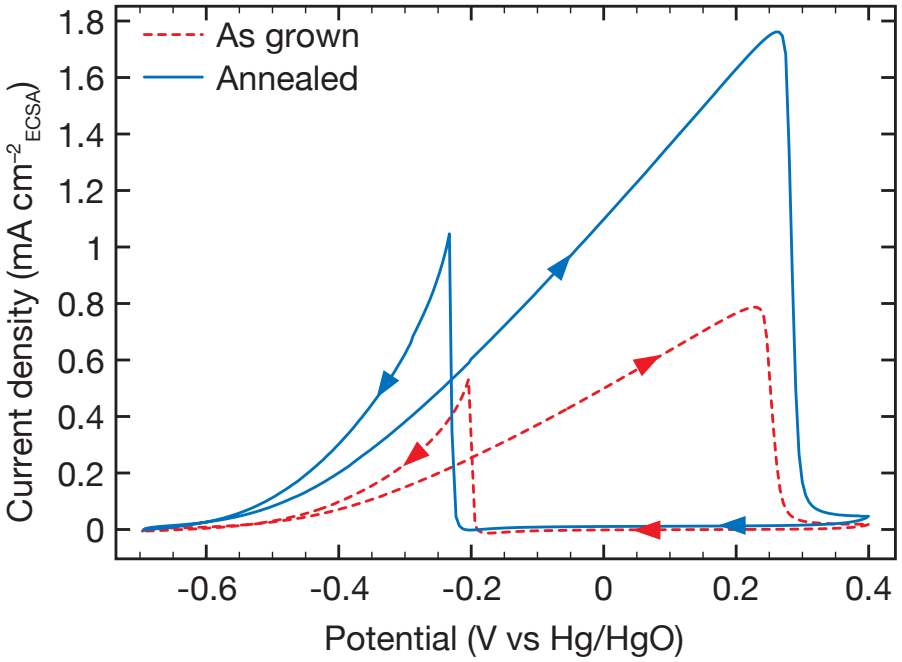

Figure 10: Cyclic voltametry of as-grown (red line) and annealed (blue line) SnO_2/TNTs after 500 Pd cycles. The electrolyte is 1 M KOH + 1 M C_2H_5OH and the scan rate is 25 mV s^{-1}.

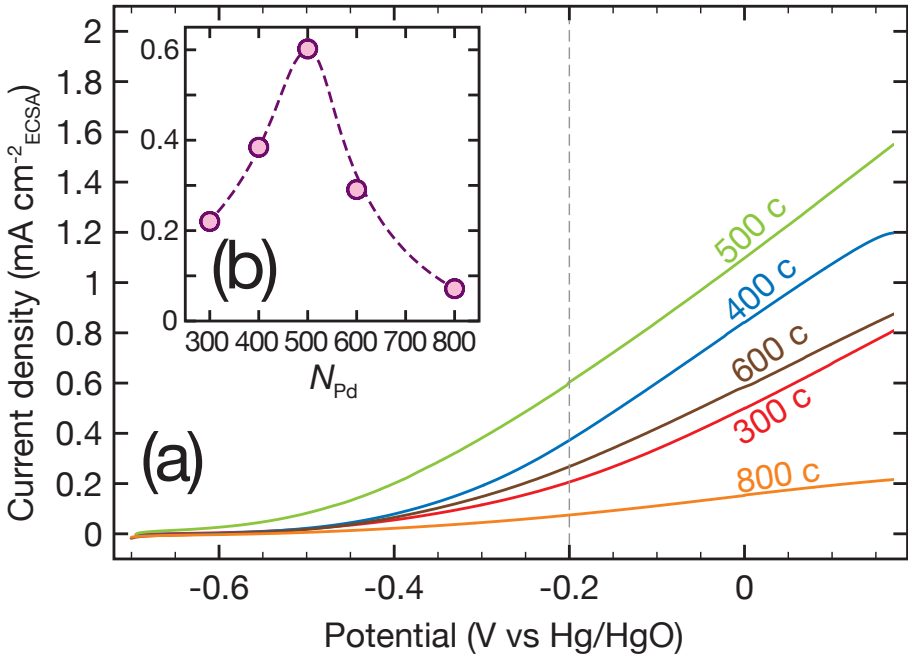

Figure 11: (a) Forward scans and (b) current density measured at –0.2 V for annealed SnO_2/TNTs after ALD of Pd for N_{Pd} = 300, 400, 500, 600 and 800 cycles. The electrolyte is 1 M KOH + 1 M C_2H_5OH and the scan rate is 25 mV s^{-1}.

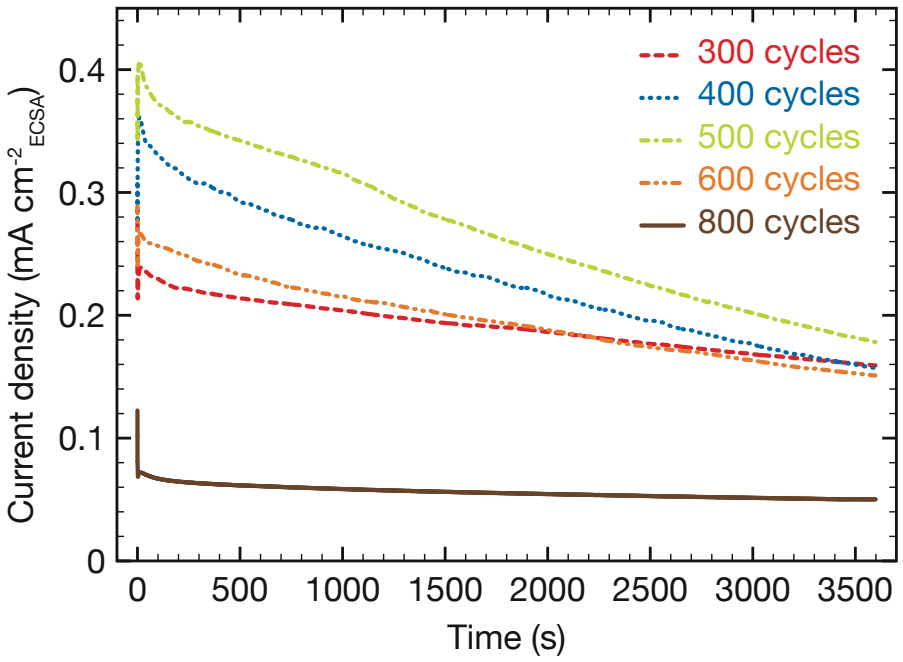

Figure 12: Chronoamperograms of annealed Pd/SnO_2/TNTs catalysts with different amount of deposited Pd, as indicated in the figure, at –0.2 V in 1 M KOH + 1 M C_2H_5OH.

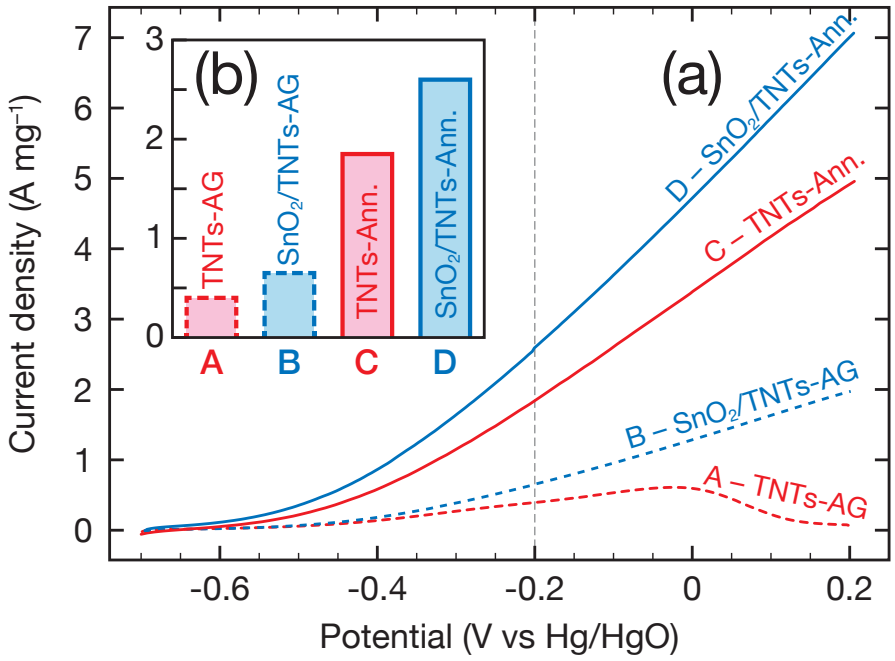

Figure 13: (a) Linear sweep voltammetry and (b) current density measured at –0.2 V for 500 cycles of Pd on as-grown TNTs, annealed TNTs, as-grown SnO_2/TNTs and annealed SnO_2/TNTs. The electrolyte is 1 M KOH + 1 M C_2H_5OH and the scan rate is 25 mV s^{-1}.

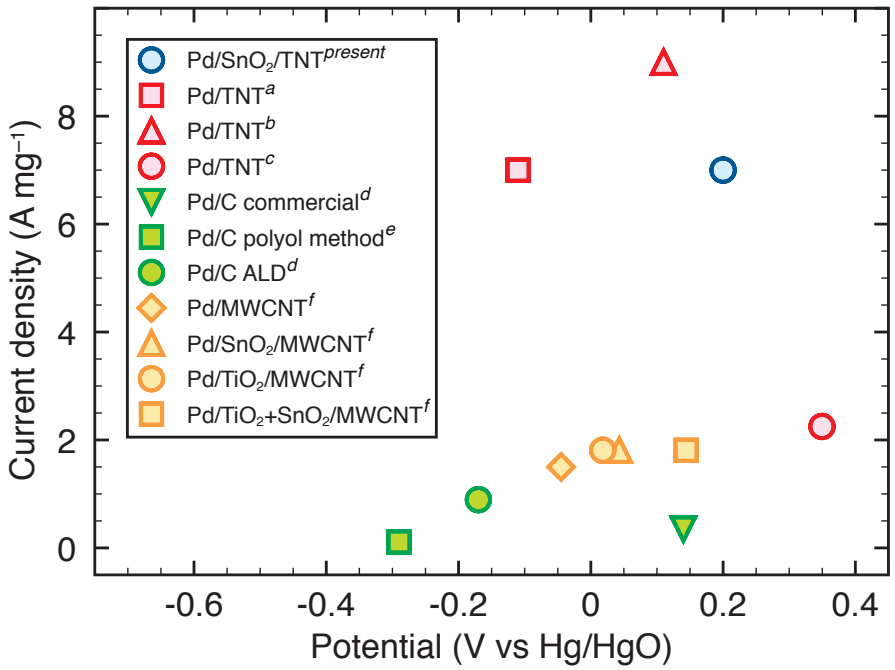

Figure 14: Comparison of the forward ethanol electrooxidation peak current and potential on Pd catalysts deposited on various types of substrates. The CVs are performed in alkaline media containing ethanol with a scanning rate ranging from 5 to 50 mV s^{-1} (see detailed information in Figure S7). Pd/TNT[a],[72] Pd/TNT[b],[70] Pd/TNT[c],[16] Pd/C commercial[d],[73] Pd/C ALD[d],[73] Pd/C polyol method[e],[74] Pd/MWCNT[f], Pd/SnO_2/MWCNT[f], Pd/TiO_2/MWCNT[f], Pd/TiO_2+SnO_2/MWCNT[f].[75]

TOC Graphic